The Characterization of Deformation Stage of Metals using Acoustic Emission Combined with Nonlinear Ultrasonics

Jennifer Vetrone, Javier E. Obregon, Ernesto J. Indacochea and Didem Ozevin*

University of Illinois at Chicago

Civil, Materials and Environmental Engineering

*Corresponding Author Email: dozevin@uic.edu, Phone: (312) 413 3051

Abstract: This paper introduces a new acoustic emission (AE) characteristic to determine the deformation stage of metals under quasi-static loading. The AE characteristic is extracted from the derivative of the cumulative AE energy with respect to time. The reproducibility of the developed feature is demonstrated on a set of A572 Grade 50 steel coupons loaded up to different levels of plastic deformation, and then evaluated using the AE data recorded from aluminum 1100. To address the prior load-dependence of AE data, nonlinear ultrasonics is studied to quantify the presence of plastic deformation as a way to determine the initiation strain during quasi-static load testing typically used for evaluating metallic structures with the AE method. The sensitivity of nonlinear ultrasonics is compared with the linear ultrasonics showing the higher sensitivity of third harmonic nonlinearity coefficient to plastic deformation. The microstructural changes affecting ultrasonics are identified with metallographic characterizations.

Keywords: acoustic emission; energy slope; deformation stage; metals; nonlinear ultrasonics; reproducibility

1. Introduction

Metals can develop inelastic deformation due to excessive loading, localized area loss due to corrosion or accidental impact due to truck. The measurement of localized plastic deformation by means of nondestructive evaluation (NDE) methods is important to understand the residual strength of structural element. Acoustic Emission (AE) is a passive NDE method, which depends on the release of elastic waves due to the progress of localized deformation. AE has been used in assessing the structural

integrity of metallic structures (Ono 2018) for detecting defects such as pressure vessels (Zou et al. 2017, Lepikhin et al. 2018, Zhang et al. 2020), bridges (Yu et al. 2011, Megid et al. 2019, Qu et al. 2020), pipelines (Juliano et al. 2013, Quy and Kim 2020). In general, AE is implemented as a diagnostic method, which detects the presence and location of defects. Without the stress history of the component, understanding acoustic emission data can be challenging. The exact conditions of a specific circumstance monitored by AE (e.g., materials composition, loading history) are difficult to replicate. The influences of background noise and experimental variables (e.g., sensor type, propagation path between sensor and source) to AE features cause additional challenges in reproducibility. Common approaches to reduce the influence of background noise are pre- or post-test filtering, denoising and pattern recognition method. Filtering and denoising with wavelet decomposition (Zou et al. 2017) introduce manipulations to AE data, which may vary depending on size of test setup, sensor selected, strain rate etc. Pattern recognition method has been applied to detecting different microstructural AE sources (Linderov et al. 2018). The method has the challenge of introducing physical meaning to cluster as there may be overlaps in AE characteristics of background noise and relevant AE signal. In this study, a new AE feature driven from the derivative of cumulative AE energy with respect to time is defined to have a characteristic AE behavior indicative of deformation stage in metals. The approach is first demonstrated on a set of samples made of A572 Grade 50 steel, and then validated further using prior data published using the sample made of Aluminum 1100. As the AE method depends on prior stress history, nonlinear ultrasonics is studied as supporting the AE behavior to determine the inelastic state of metallic samples. The combination of two methods is proposed to identify the deformation state of metals.

2. Background Literature

2.1. AE Applications to Detect Plastic Deformation

As a material is strained, a localized deformation within the material rapidly releases energy and creates transient elastic waves, i.e., acoustic emission, with distinct characteristics representing the source mechanisms (Joseph and Giurgiutiu 2020). Elastic an elastoplastic deformation in metals can produce AE sources (Makhutov

2019). The origins of AE sources can be macroscopic or microscopic. Crack growth and corrosion are classified as macroscopic origin AE sources. Dislocation movement, phase transformation, and micro cracks can be considered as microscopic origin AE sources in metals (Takemoto et al. 2017, Merson et al. 2019). As plastic deformation occurs, acoustic emission sources are a result of dislocation motion and twinning in the microstructure (Bohlen et al. 2004). The stress waves propagate through the material and reach the surface where the AE sensors detect and convert a mechanical wave into an electrical signal, known as AE signal. The literature shows that cumulative AE features obtained from metals loaded under quasi-static loading have a characteristic behavior such that AE hit rate increases until the beginning of plastic deformation and then slows down in strain hardening and necking regions (Penkin et al. 2017, Petit et al. 2018, Botvina and Tyutin 2019, Kietov et al. 2019). Su et al. (2018) concluded that the AE signal intensity can be used to determine the yielding point of metals. Zou et al. (2017) introduced the ratio of energy between two frequency ranges to predict the deformation stage. Vinogradov et al. (2019) applied the AE power and the AE median frequency to describe the plastic deformation in metals. However, the AE data depends on prior stress history and the direct use of AE features depends on the AE sensors and setting as well as sensor-source spacing (Aggelis and Matikas 2012). Additional information and reference-free AE feature are needed to identify the deformation state. The correlation of damage mechanisms with the AE characteristics can be built if numerical simulations are built with considering all the details of sources and data acquisition variables (La Gall et al. 2018).

2.2. NLUT Applications to Metals

Nonlinear ultrasonic testing (NLUT) based on the detection of higher harmonic signals is an active NDE method that is based on detecting the generation of higher harmonics in materials when the fundamental harmonic signal interfaces with heterogeneities in the medium. NLUT is a powerful NDE method because it correlates the mechanical properties of a material with the characteristics of wave propagation in subwavelength (Li et al. 2019). The method has been successfully applied to different metallic alloys (Lissenden et al. 2020, Kamali et al. 2019, Mostavi et al. 2017). The generation of high harmonics can be attributed to many sources inside the material. These sources include

lattice defects such as voids, vacancies, precipitates, grain boundaries, dislocations, and microcracks. Heterogeneities in the material can be correlated with higher harmonics using the acoustic nonlinearity parameters β and γ , which are calculated from the amplitudes of the fundamental, second-, and third-harmonic frequency components (Kamali et al. 2019). When a solid medium is excited with plane wave as $u(0,t)=u_0\sin\omega t$, the solution considering higher order terms in the strain energy produces the following displacements at different positions, x (Solodov 2020):

$$u(x,t) = u_0 \sin \omega \left(t - \frac{x}{c_L} \right) + \frac{\beta}{8} k^2 u_0^2 x \cos 2\omega \left(t - \frac{x}{c_L} \right) + \frac{\gamma}{24} k^3 u_0^3 x \sin 3\omega \left(t - \frac{x}{c_L} \right)$$

$$+ \cdots$$

where c_L is longitudinal wave velocity, β is acoustic nonlinearity coefficient, k is wave number, ω is ultrasonic circular frequency. The equation can be rewritten considering only the first three terms as

$$u(x,t) = A_1 \sin \omega \left(t - \frac{x}{c_L} \right) + A_2 \cos 2\omega \left(t - \frac{x}{c_L} \right) + A_3 \cos 2\omega \left(t - \frac{x}{c_L} \right)$$
 (2)

 A_1 , A_2 and A_3 are the amplitudes of the first (ω) , second (2ω) and third (3ω) harmonic waves. Material nonlinearity generates the second-harmonic and the second-order acoustic nonlinearity parameter β can be quantified by the following relationship:

$$\beta = \frac{8A_2}{A_1^2 \times k^2} \tag{3}$$

In NLUT experiments for the second harmonic nonlinearity, A_1 , and A_2 are indirectly measured as A_1 and A_2 , which are the fundamental and second harmonic amplitudes extracted from Fourier transform of time domain histories detected by an ultrasonic transducer. Equation 3 is re-written as

$$\beta' = \frac{A_2'}{A_1^2 x} \tag{4}$$

In this equation, β is proportional to β . As wavenumber is constant, it is embedded in the β calculation. Since the magnitudes of the harmonic waves are dependent on the

medium's material nonlinearity, the second order harmonic characterizes the nonlinearity of a material.

Correspondingly, the third-order acoustic nonlinearity parameter is defined using the first and third harmonic terms in equations 1 and 2 as

$$\gamma = \frac{24A_3}{A_1^3 \ xk^3} \tag{5}$$

Similarly, for the third harmonic nonlinearity, A_1 , and A_3 are indirectly measured as A_1 and A_3 , which are the fundamental and third harmonic amplitudes extracted from Fourier transform of time domain histories detected by an ultrasonic transducer. Equation 5 is re-written as

$$y' = \frac{A'_3}{A'_1^3 x} \tag{6}$$

Heterogeneity in materials can be quantified using the second- and third-order nonlinearity parameters since these parameters are directly related to A_1 , A_2 , and A_3 (Kamali et al. 2019). Microstructural damage due to creep, fatigue, aging, and thermal damage can be identified using nonlinear ultrasonics. Fatigue damage can be characterized by nonlinear ultrasonics using the nonlinear ultrasonic parameter β . The parameter was determined to increase monotonically with hardness and carbon content over a range of 0.1-0.4 mass% (Jhang 2009). Jhang and Kim (1999) studied the nonlinear ultrasonic parameter's response to increasing tensile stress in structural steel. With increasing tensile stress, the nonlinear ultrasonic parameter increased, and was especially sensitive to change when the tensile stress applied became larger than the yield stress. A study by Viswanath et al. (2011) found that in AISI type 304 stainless steel, β was found to increase when the steel underwent cold work due to an increase in dislocation density, the formation of dislocation double walls, and the formation of martensite.

2.3. Knowledge Gap

The current studies on measuring the deformations stage with the AE method are based on absolute AE values, which depend on the measurement setting (e.g., sensor selected, threshold, timing variables, filters). Additionally, the dependence of AE feature plots on prior deformation stage has not been addressed. In this study, a characteristic

AE behavior representing the plastic deformation stage in metals is built independent from testing variables and microstructural variability. We demonstrated a reproducible AE characteristic representing the deformation stages in different metals. NLUT is studied to detect the amount of inelastic deformation in A572 Grade 50 steel such that the prior stress history can be predicted to understand the initiation point on the stress-strain curve supporting the AE results.

3. Materials Preparation and Experimental Setup

3.1. Materials Preparation

A572 grade 50 high-strength low-alloy (HSLA) steel with chemical composition limits given in Table 1 was used to build the coupons as shown in Figure 1. Ten coupons were machined from as received ¼ inch thick plate according to ASTM standard E8 and milled down to 6 mm thickness. The samples were stress relieved at 400°C for 30 minutes prior to testing and the furnace used for the stress relief.

Table 1. Chemical composition limits of A572 Grade 50 HSLA steel used to build the coupons (ASTM A572/A572M-18).

Element	С	Mn	Р	S	Nb	V	Ti	N	Fe	
Weight %	0.23	1.35	0.03	0.03	0.015	0.15	0.04	0.015	Bal.	

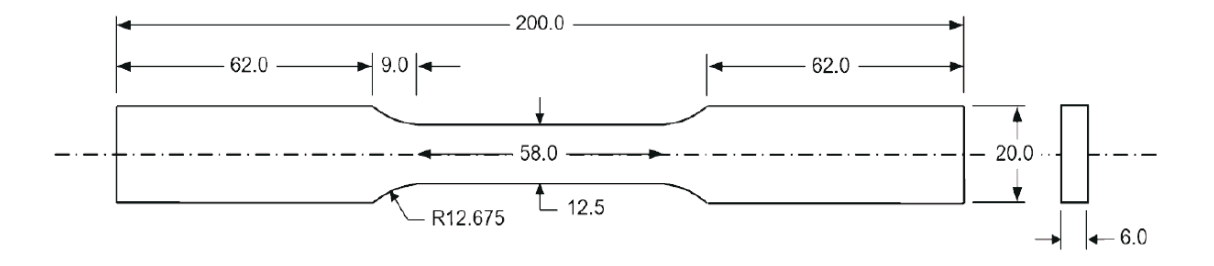


Figure 1. Materials composition and dimensions of A572 Grade 50 coupons in mm.

The samples were plastically deformed to different strains beyond the yield stress using uniaxial loading. An MTS tensile machine, model 1125 was used for tensile testing at a strain rate of 2.54 mm/min. To determine the true yield strength and tensile strength, the first sample was loaded to failure. The remaining samples were loaded until the specified elongation was reached as shown in Figure 2c and d.

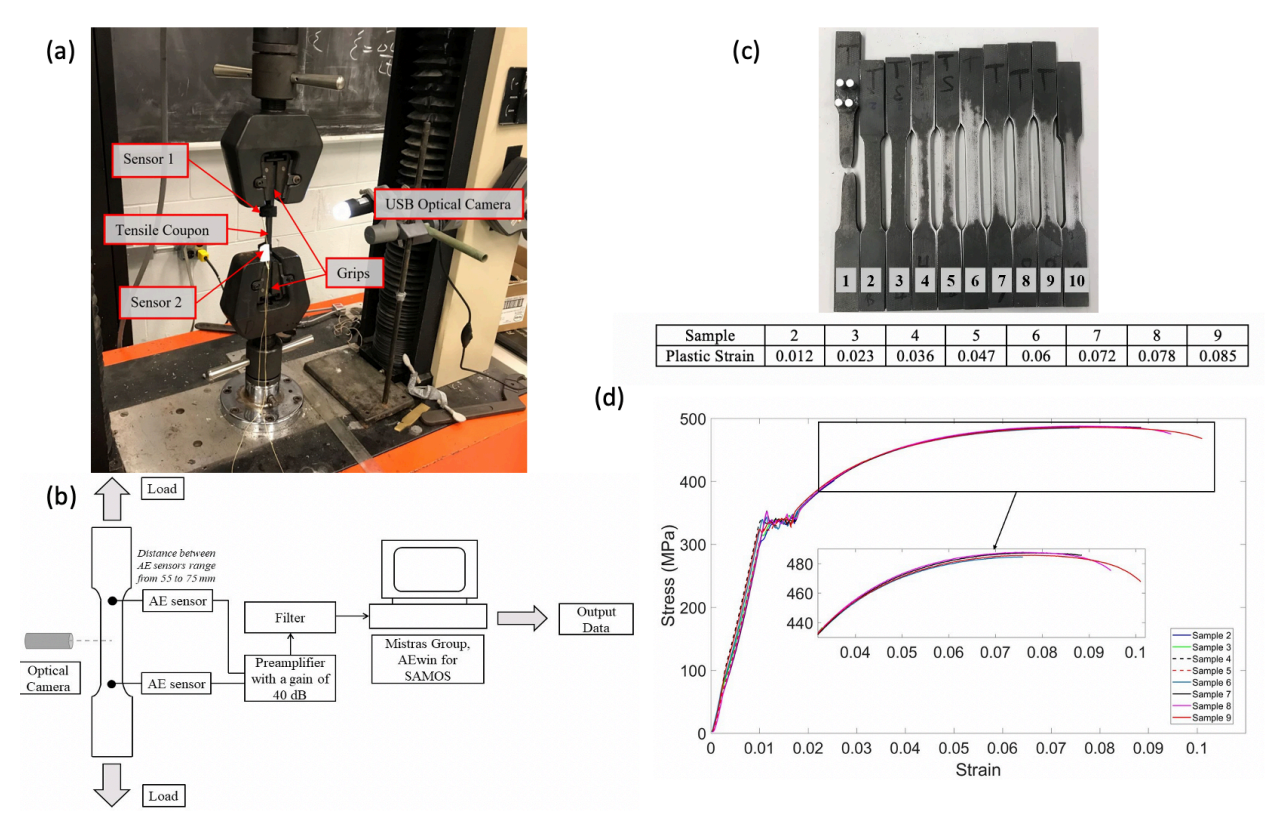


Figure 2. Sample design with different plastic deformation levels, (a) experimental setup, (b) AE schematic, (c) samples at post-loading with the final recorded plastic strains and (d) strain-stress curves of eight samples.

2.2 NDE Measurements

Four NDE methods were used to assess the plastic deformation of samples as shown in Figure 3. The specifications of methods are as follows:

Method 1: The AE method was applied as an *in situ* and real-time assessment method assisted with an optical microscope to detect the damage progression. Two nano 30 sensors (manufactured by Physical Acoustics) were attached using vacuum grease and securely positioned using electrical tape. Nano 30 sensor has the operation frequency range of 125-750 kHz with resonance frequency near 300 kHz. The threshold was set as 40 dB to minimize the influence of extraneous noise sources. The data acquisition setting included a threshold of 40 dB, analog filter of 100-400 kHz, and sampling rate of 1 MHz. Timing variables were hit driven time as 800 μ s, hit lockout time as 1000 μ s, and peak definition time as 200 μ s. The AE features extracted were rise

time, counts to peak, counts, energy, duration, amplitude, average frequency, signal strength, absolute energy, centroid frequency, peak frequency, channel, partial power 1, partial power 2, partial power 3, and partial power 4. Typically, the frequency domain features including centroid frequency, peak frequency and partial powers are used for source classification. AE amplitude is applied for understanding the intensity of AE source. Temporal AE features including rise time and duration are affected by the rate of AE energy, the source energy, threshold and timing parameters. The cumulative AE energy is a good indicator of loading history especially for quasi-static loading. However, as its absolute value depends on experimental variables, a new feature of the derivative of the cumulative acoustic emission energy over time is introduced in section 4.1 to minimize the influence of experimental variables.

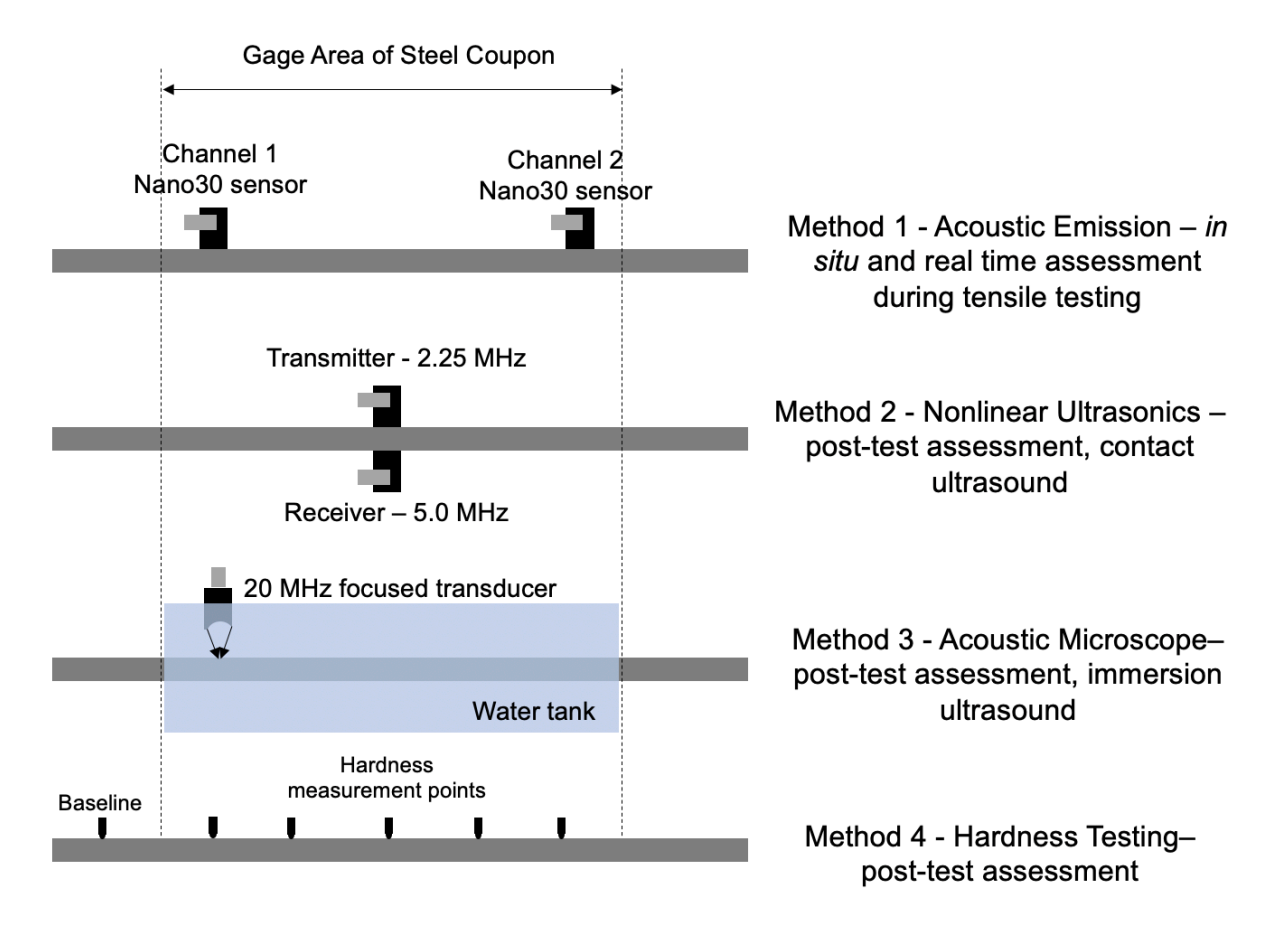


Figure 3. Summary of NDE measurements from the coupons.

Method 2: After the samples were loaded to different levels of plastic deformation, they were unloaded and assessed using nonlinear ultrasonics. A 2.25 MHz transmitter and

5.0 MHz receiver were used in the NLUT experiment. The transmitter as 5 MHz has the bandwidth of 3.28-7.67 MHz to capture the second and third harmonics of 2.25 MHz fundamental frequency (Kamali et al. 2019). The sensors were glued to a weighted clamp facing each other. A weighted clamp was used to provide constant pressure and a light lubricant oil couplant was applied to the surfaces of the sensors. Before each measurement, the specimen and the sensors were cleaned of any oil and the sensors were lubricated again. A tabletop UT machine was used with an input signal of a 10-cycle, 300-voltage, tone burst at 2.25 MHz. Before tensile testing, three measurements were taken in each of the five sections on the sample. After tensile testing, three measurements were conducted in the center of the gage length and averaged. On samples 8 and 9, visible necking regions occurred because of the tensile test. As a result, three measurements were taken on the neck and directly outside the necking region to capture material nonlinearity in both areas.

Method 3: A Sonoscan Gen6 C-mode Scanning Acoustic Microscope was used for immersion ultrasound experiments on the samples. Three scans were performed with the focus on the gage length. A 20 MHz ultrasonic transducer with a 3.81 cm focal length and a 13.31 mm depth of focus was used and focused on the back surface of the sample.

Method 4: Rockwell B hardness testing was performed using a 0.42 cm diameter indenter. Before tensile testing, four hardness measurements were taken for each sample outside the gage and shoulder region. After tensile testing, hardness tests were performed on each sample with the same procedure but with indentation occurring in the gage length. Five measurements were taken in the gage length.

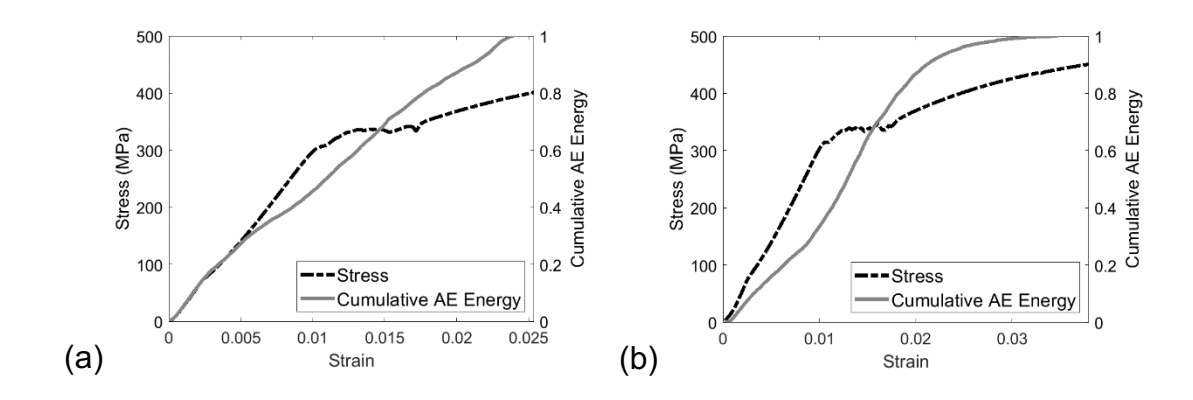
4. Experimental Results

4.1. Construction of Normalized Energy Curves from AE Data

While the stress-strain curves exhibit excellent repeatability, the AE data shows significant variability due to the complexity in measurement and the influence of many factors in generating AE signal. In terms of measurement factors, the AE data is influenced by how AE sensors are attached to the surface. While they were attached with the same method, it is not possible to reach to exact surface condition. It is noticed

during experiments that heat treatment to release machining stress caused the development of oxide layer, which started to break during loading leading to the release of AE signals. The oxide layer was removed from samples 6 to 9, which influenced the absolute characteristics of AE data. Therefore, a unified approach considering the variability in AE data to predict the level of plastic deformation using the AE data is needed.

Cumulative acoustic emission energy is shown with a solid grey line and the stress is graphed with a dashed black line in Figure 4. Samples 2, 3, 4 and 5 had the oxide layer still present on the surface of the samples during testing and samples 6, 7, 8, and 9 had the oxide layer removed. For the samples that had the oxide layer removed, the acoustic emission energy curve closely follows the stress-strain curve. For samples with the oxide layer present on the surface during testing, the cumulative acoustic emission energy does not show drastic or distinct changes contrary to the samples with the oxide layer removed. The oxide layer breakage was detected by the acoustic emission sensors as a secondary emission source in addition to plastic deformation that produced AE activity during the tensile test. Evident in Figure 4a through Figure 4d, the cumulative acoustic emission energy curve is more gradual because of the secondary emission source and indicates the negative effect of secondary emission to AE data.



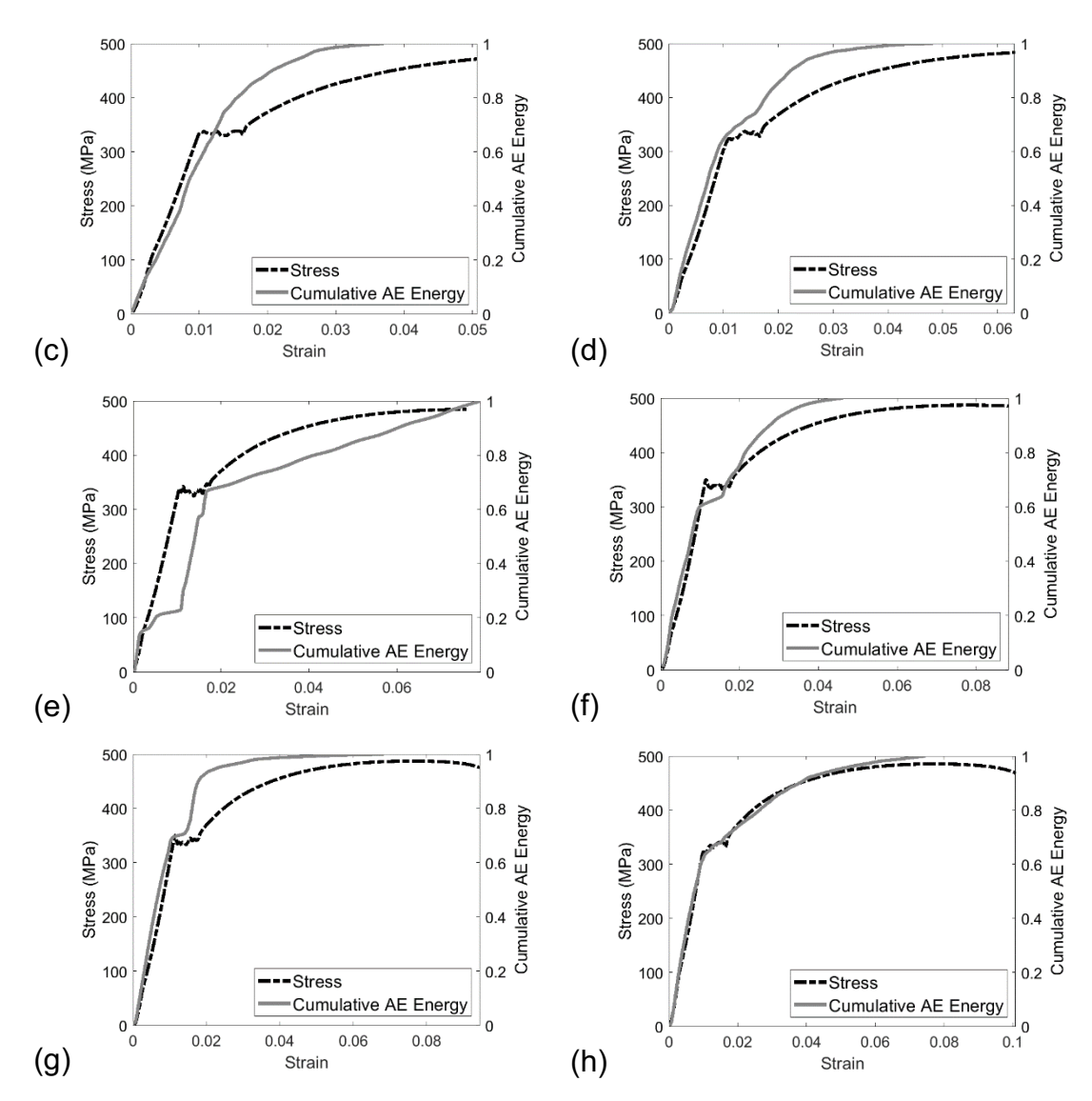


Figure 4. The evolution of cumulative AE energy with respect to stress for (a) sample 2, (b) sample 3, (c) sample 4, (d) sample 5, (e) sample 6, (f) sample 7, (g) sample 8, and (h) sample 9.

With the reduced influence of the oxide film, samples 6 through 9 have cumulative AE energy curves that closely follow the corresponding stress-strain curves, seen in Figure 4e through Figure 4h. The curve has a sudden increase at the initial phase due to AE signals generated by the initial loading and stress release. The increase in AE energy slows down in the plastic regime and then exhibits a nonlinear increase in the strain hardening phase. The cumulative AE activity becomes inactive in the necking region, that indicates localized deformation.

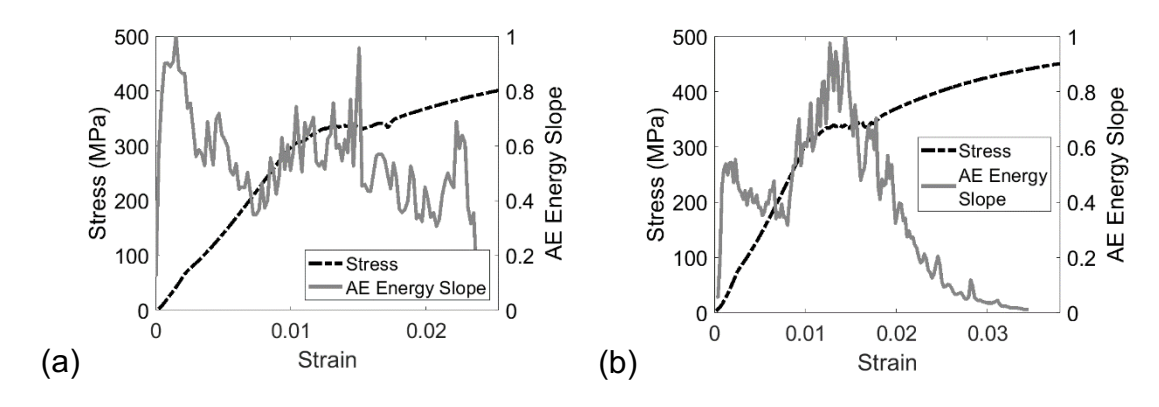
To further understand the acoustic emission energy, the discrete derivative of the cumulative acoustic emission energy over time was calculated. First, the length of each time vector per sample was spaced evenly by one second. The acoustic emission energy data was then interpolated for each index in the corresponding time vector between the two nearest recorded acoustic emission points described as follows:

$$\Sigma A E_{energy}(n) = A E_{energy}(n) + \Sigma A E_{energy}(n-1)$$
(7)

where n is the vector index as n=1 ... length(AEdata). AE_{energy} is the acoustic emission energy at the vector index n. The cumulative AE energy, ΣAE_{energy} , is normalized to the maximum value that the data acquisition system can capture, which is 65,535. The slope of cumulative AE energy is calculated by

$$ES(n) = \frac{\sum AE_{energy}(n) - \sum AE_{energy}(n-1)}{t(n) - t(n-1)}$$
(8)

where ES(n) is the acoustic emission energy slope and t is time. The acoustic emission energy slope is graphed with respect to stress in Figure 5. In samples 2 through 5 (Figure 5a-d), the cumulative AE energy slope does not show significant changes in behavior and it is large at the beginning and decreases throughout the test. For samples 6 through 9 (Figure 5e-f), the cumulative AE energy slope is very high before the yield point. After the yield point, the AE energy slope decreases significantly and plateaus. The AE energy slope then increases after the yield plateau in the strain hardening region of the stress-strain curve and decreases for the remainder of the plastic region. The AE slope data for samples 6 through 9 have defined regions of behavior synonymous with the stress-strain curve visible in Figure 5e through Figure 5h.



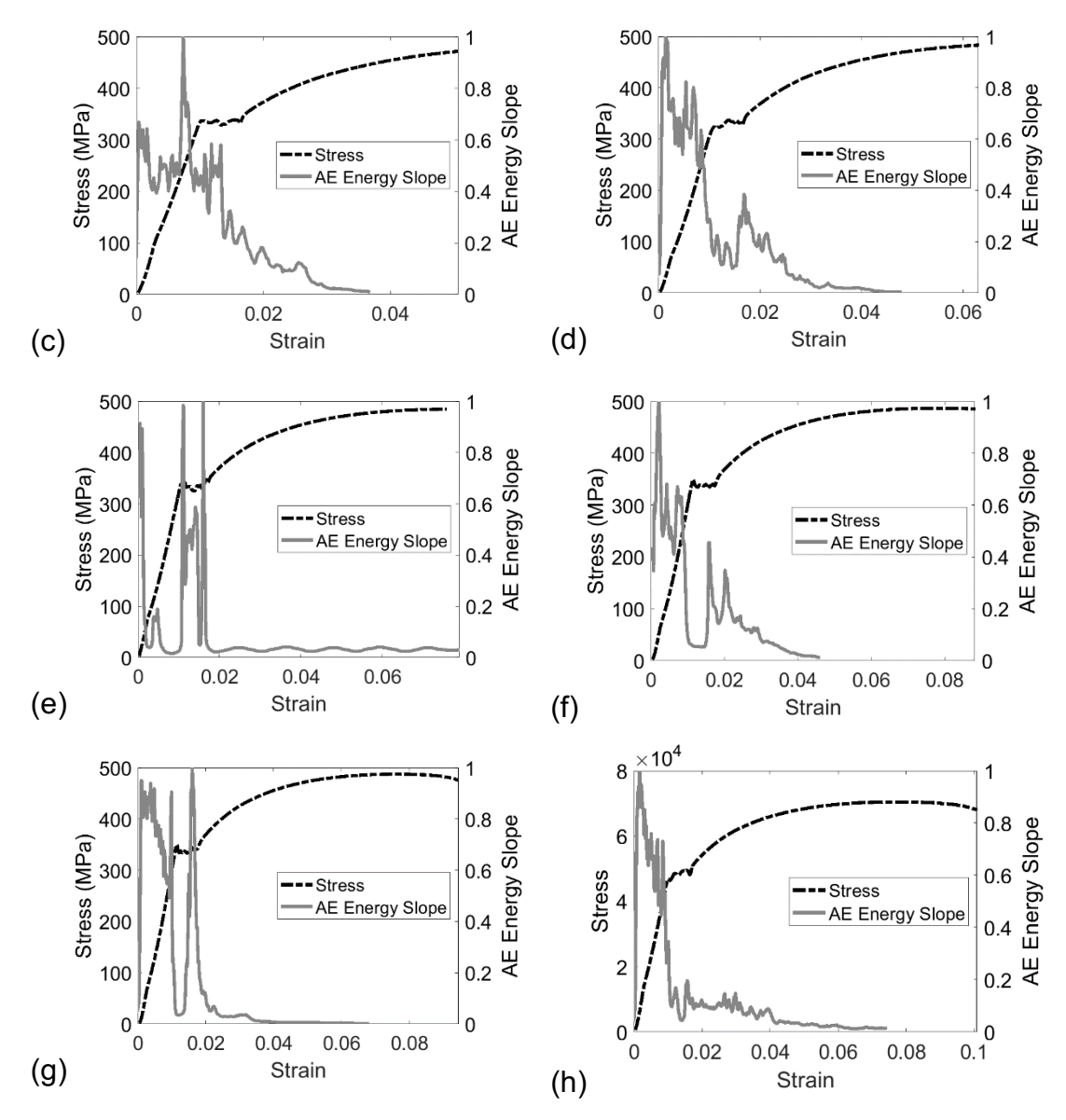


Figure 5. The progression of the AE energy slope graphed with stress for (a) sample 2, (b) sample 3, (c) sample 4, (d) sample 5, (e) sample 6, (f) sample 7, (g) sample 8, and (h) sample 9.

During the plastic zone, massive dislocations most likely occur causing a large AE response. As strain increases, the density of dislocation walls increases causing the AE activity to drop. This is consistent in Figure 5e through Figure 5h, as once the strain hardening region is entered, the AE count rate drops dramatically.

The AE energy slope is divided into five deformation stages as shown in Figure 6. During the initial loading, stress release causes a significant jump in the AE energy slope, which plateaus at the linear elastic stage. An increase in the AE energy slope

occurs in the plastic region supporting massive dislocation movements (Lyasota et al. 2019). A negative slope defines strain hardening region, which is reduced further at the necking region.

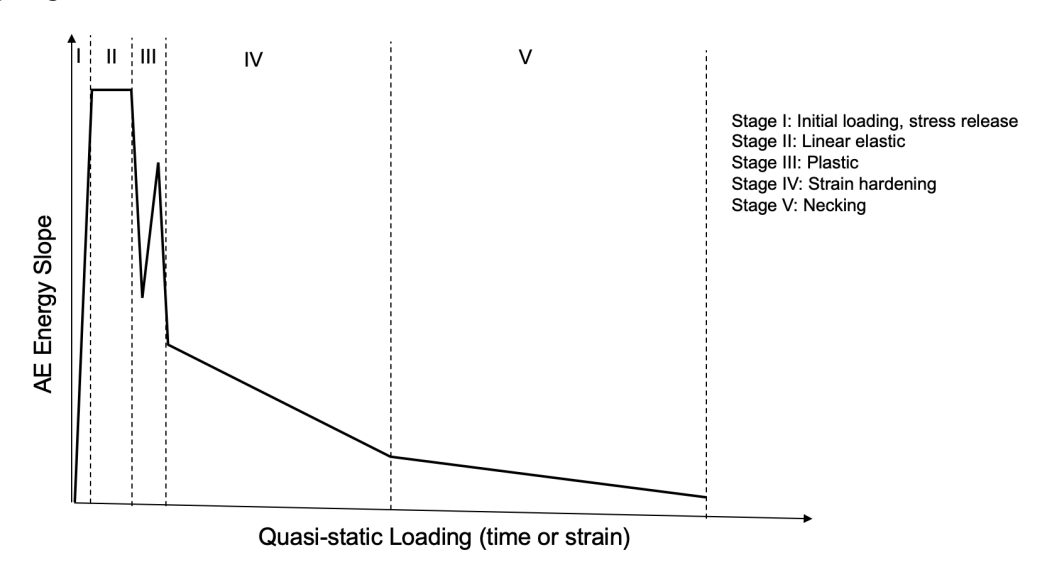


Figure 6. AE characteristic of AE energy slope as an indicative of metal deformation under quasi-static loading.

To demonstrate the reproducibility of the AE energy slope behavior, equations 7 and 8 were applied to another data set reported by Zhang et al. (2018). The sample dimensions (following ASTM E8), pre-preparation (stress relief via heat treatment), sensor attachment (vacuum grease) and loading (quasi-static with 0.04 mm/s rate) were similar to the ones applied to A572 Grade 50 steel samples presented in Figure 5. The differences between two tests were materials (Aluminum 1100) and AE sensors (WD sensors).

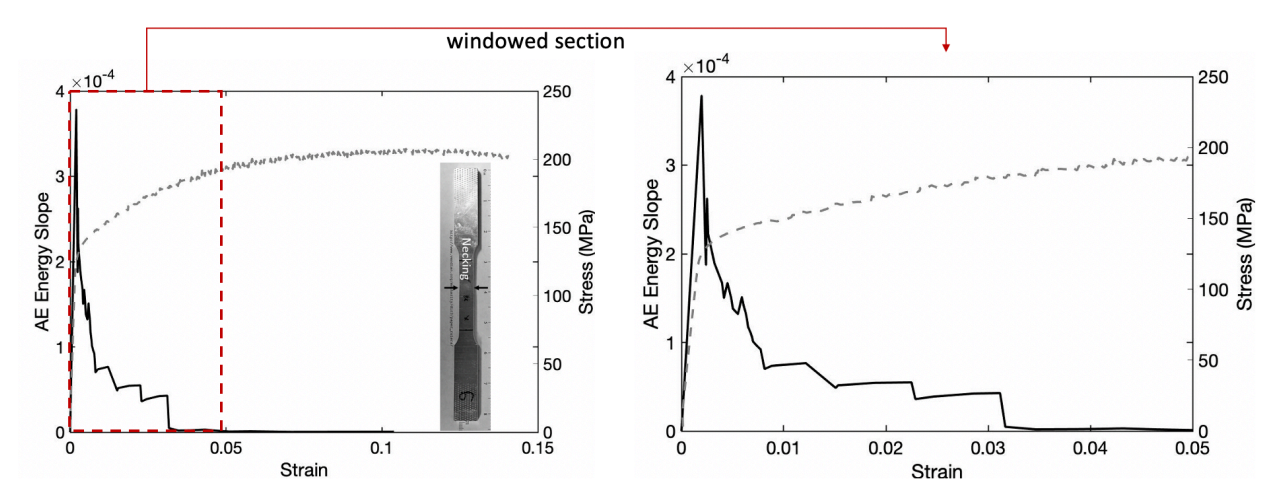


Figure 7. Reproducibility of AE result on aluminum 1100 sample.

Figure 7 shows the AE energy slope of the data recorded from aluminum 1100 without applying any post-processing filter. As the sample does not have a well-defined yielding plateau as steel, the transition between linear elastic and yielding is not clear. However, the windowed section indicates a sharp increase in the AE value between elastic-inelastic stages and negative slope at hardening section, which shows the reproducibility of AE energy slope characterized in deformation stages shown in Figure 6.

4.2. Nonlinear Ultrasonics (NLUT) Results Combined with Hardness Measurement and Acoustic Microscopy

Understanding the microstructural deformation prior to typical load testing of AE is important. NLUT was utilized for detecting whether the material had been exposed to inelastic deformation. The time history waveform recorded during the nonlinear ultrasonic test was transformed from amplitude vs. time to amplitude vs. frequency graphs using FFT (Fast Fourier Transform). Stable windows representing harmonic behavior were chosen for each sample based on constant amplitudes for approximately 6 cycles. The amplitude vs. time and voltage vs. frequency graphs for sample 6 are shown in Figure 8a and Figure 8b, respectively. The fundamental, second-, and thirdorder harmonic amplitudes were recorded for each sample from the FFT conversion graphs. Since the acoustic nonlinearity parameters are dependent on sample thickness, the thicknesses of each sample were measured three times with a caliper in the same location that nonlinear ultrasonic measurements were taken and averaged. Acoustic nonlinearity parameters β' and γ' were calculated using equations 4 and 6, respectively. The second- and third-order harmonic nonlinearity coefficients were graphed with the sample hardness after tensile testing and the final recorded strain for each sample in Figure 9a and Figure 9b, respectively.

Deleted:

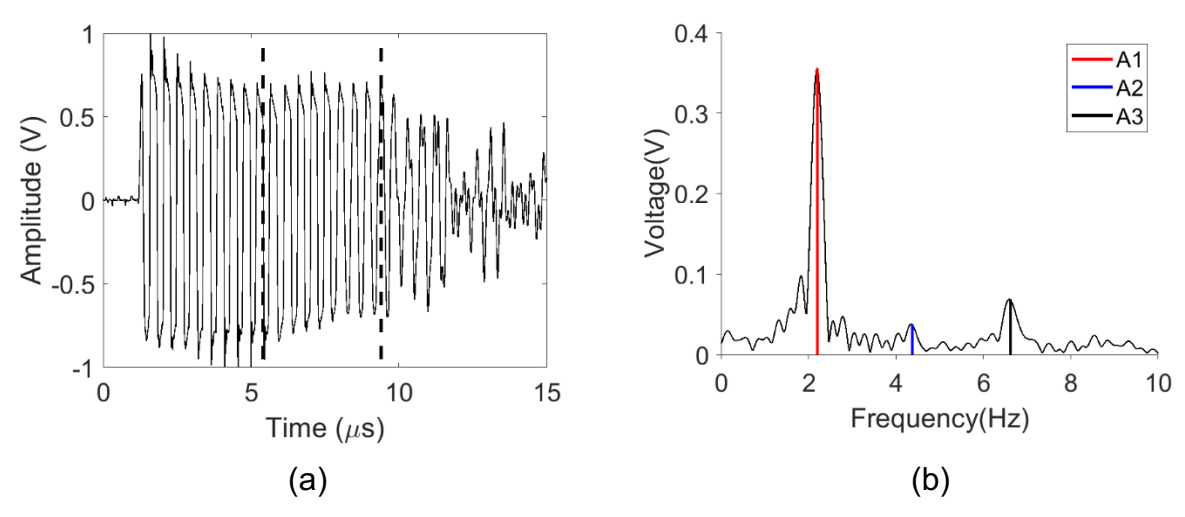


Figure 8. Nonlinear ultrasonic testing results for sample 6 with the (a) time history waveform and the selected window size shown in black dashed lines and (b) the FFT result with the fundamental amplitude, A_1 , labeled in red, the second-order harmonic amplitude, A_2 , in blue, and the third-order harmonic amplitude, A_3 , in black.

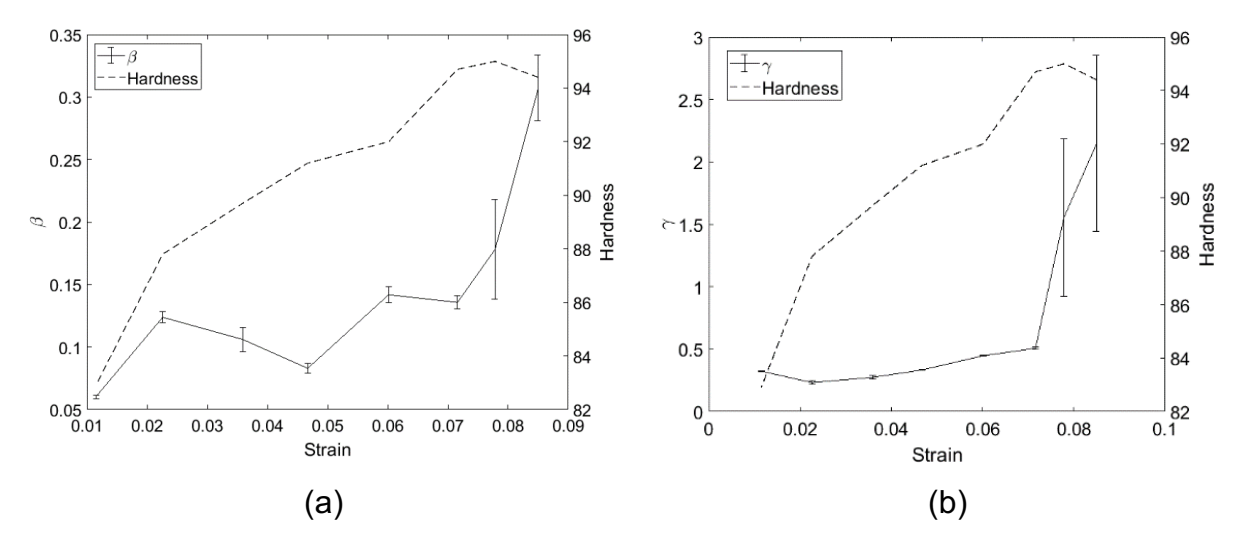
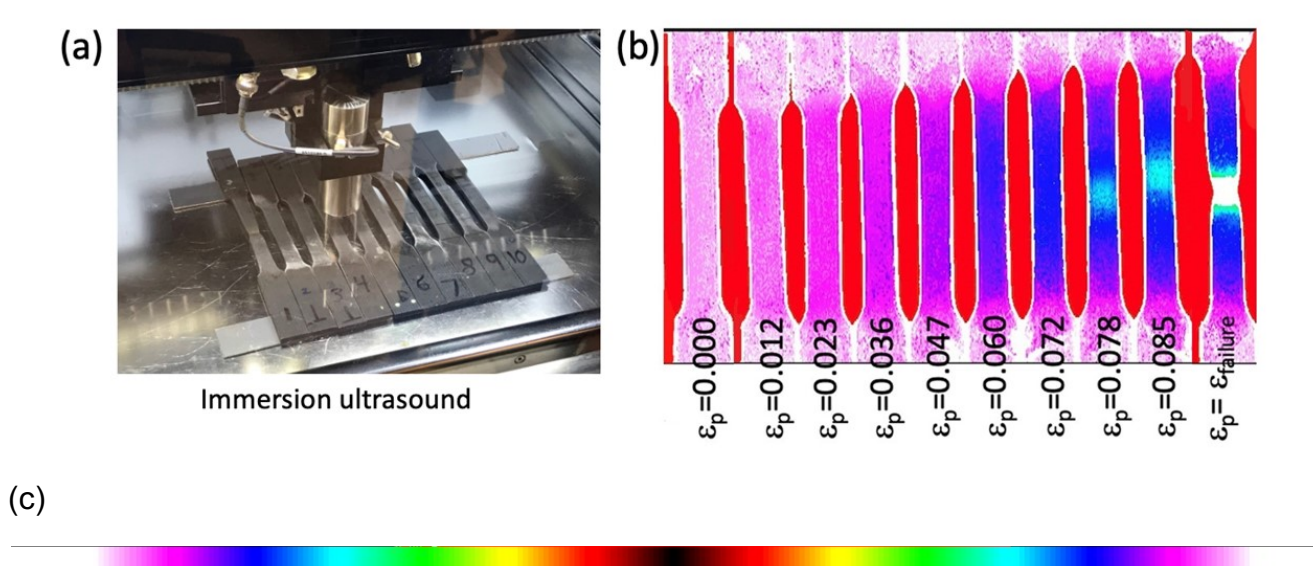


Figure 9. Variation of the nonlinearity coefficients with the plastic deformation and hardness (HRB), (a) the second harmonic nonlinearity coefficient, (b) third harmonic nonlinearity coefficient.

From the second sample to the ninth sample, the second- and third-order harmonic nonlinearity coefficients increase by 411% and 565%, respectively. An increasing trend is seen primarily with the third harmonic nonlinearity coefficient. Nonlinear ultrasonic measurements for samples 8 and 9 were taken specifically in the necking regions of the samples; these two samples were the only samples that displayed prominent necking regions. Samples 8 and 9 have large third harmonic and second harmonic nonlinearity coefficients due to the high amount of plastic deformation.

The bulk scan measurement with the acoustic microscope using 20 MHz transducer is shown in Figure 10. The samples were tested concurrently inside the water basin. The linear ultrasonics indicates the thickness change as a result of plastic deformation after the plastic deformation reaches 0.047. While relatively high ultrasonic frequency is selected, linear ultrasonics cannot detect the plastic strain until it reaches 0.047 as compared to NLUT. The development of necking in samples with the plastic deformation above 0.078 is clearly seen. Necking causes non-flat surface, which negatively influences the NLUT measurement using contact transducers. This explains the significant fluctuations observed in the third harmonic nonlinearity coefficient shown in Figure 9b. The comparison of linear ultrasonics (Figure 10) and nonlinear ultrasonics (Figure 9b) shows the higher sensitivity of the third harmonic nonlinearity coefficient to the plastic deformation.



-100% 0% 100%

Figure 10. Acoustic microscope results, (a) samples lined in the acoustic microscope after they underwent tensile testing, (b) C-scan image using time of flight from back surface, (c) acoustic microscope scale

Metallographic characterization was performed to describe the changes in microstructure leading to the nonlinearity in ultrasonic signal. The metallographic characterization at the end of Sec 4.2 was performed following ASTM standard E3-11. Samples were cut in the longitudinal and axial directions, placed into epoxy molds, and polished according to ASTM E3-11. They were grinded using silicon carbide paper from

grit 180 and up to grit 1200. Fine polishing was done in two stages: first with alumina suspension with particle size of 1 micron, and second with alumina suspension with particle size of 0.05 microns. Finally, samples were clean with DI water and then with ethanol. The samples were etched with a 2% nital solution. The cross section and longitudinal direction at 500X are shown in Figure 11, and Figure 12, respectively. The increasing grain elongation is visible in the photographs in the longitudinal direction. Elongated grains are especially visible in Figure 12h and i showing samples 8 and 9's microstructure. Sample 9 underwent the most elongation, and visible differences in grain diameter can be seen when comparing sample 9 with the other samples.

(a) (b) (c) (e) (d) (f) 25 µm (g) (h) (i)

Deleted:

Deleted:

Figure 11. Cross section of the sample microstructure at 500X magnification for (a) sample 10 (pristine), (b) sample 2, (c) sample 3, (d) sample 4, (e) sample 5, (f) sample 6, (g) sample 7, (h) sample 8 and (i) sample 9.

The cross-sectional images show consistent results and no changes in grain elongation because the images were taken perpendicular to the direction of loading. The grain diameter increases with increasing strain. The largest increase in grain diameter occurred in sample 9 with a 97.6% increase. The calculation of volume fraction of pearlite for the samples using ImageJ shows consistent values across numbers. Since there is no phase change after the tensile test, consistent volume fraction is expected. It is concluded that the NLUT is affected by grain size changes due to the plastic deformation.

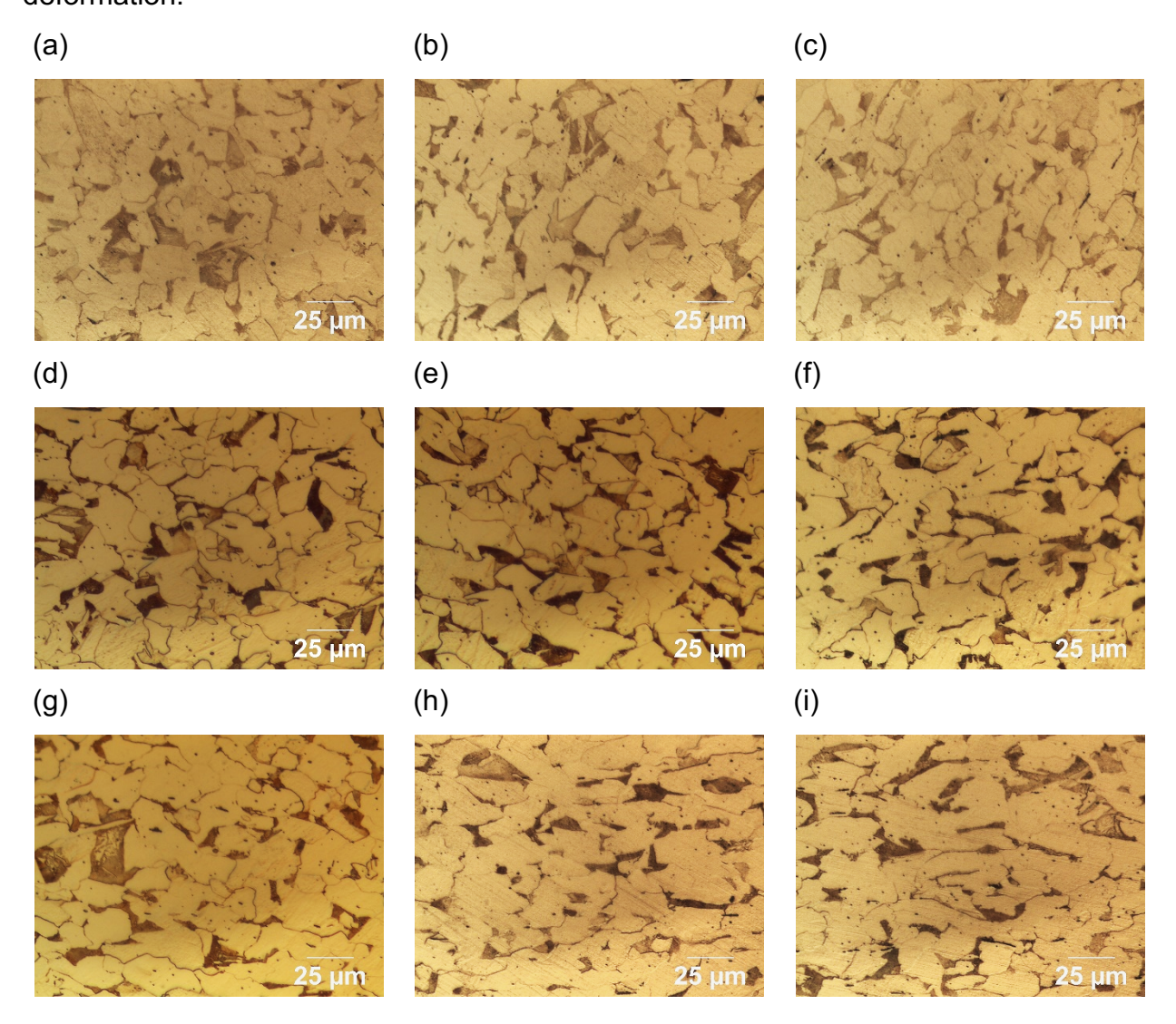


Figure 12. Longitudinal direction of the microstructure at 500X magnification for (a) sample 10 (pristine), (b) sample 2, (c) sample 3, (d) sample 4, (e) sample 5, (f) sample 6, (g) sample 7, (h) sample 8 and (i) sample 9.

5. Conclusions

Metals can be exposed to a range of deformation in their service life. The structures under constant loading, such as pressure vessels and bridges, can reach to inelastic stage. Distinct changes in acoustic emission energy were found to correspond well with regions of the tensile test stress-strain curve. Large initial changes in AE energy were found before the yield point followed by a significant decrease and a plateau close to zero during the yield plateau, because of the nonuniform strain (discontinuous yielding) typical of low carbon steels. After the yield plateau, there was a sharp increase in the change of acoustic emission energy before a decrease in energy for the remainder of the test. These changes in energy indicated that the stages of elastic and plastic deformation incurred by the sample corresponded with acoustic emission energy changes. In this study, a new AE feature, namely the AE energy slope, was introduced to identify the deformation stage of metals loaded quasi-static independent from experimental variables. The reproducibility of AE characteristics was demonstrated with two different metals. To support the AE results dependent on prior stress history, nonlinear ultrasonic testing was implemented for detecting inelastic deformation prior to loading. The testing provided fundamental, second and third harmonic amplitudes that were used to calculate nonlinearity parameters. The acoustic nonlinearity parameter using the third harmonics increased dramatically and was particularly sensitive to plastic deformation. The responses of the AE and NLUT methods to the level of quasi-static loading are different. As the AE method is a passive NDE method, the rate of AE activity is the highest at the yielding stage due to large amount of dislocation movement and the lowest at the strain hardening stage due to the restricted dislocation motion. On the other hand, as the total amount of dislocation is the highest for the samples loaded up to higher strains, the acoustic nonlinearity coefficients obtained from NLUT measurement increase. The combination of AE and NLUT can be utilized to identify the prior and post deformation stage in evaluating the structural integrity of metallic structures.

Acknowledgment

This work was partially supported by the National Science Foundation under Award No. CMMI 1914663 entitled "Conformal Gradient-Index Lenses for Ultrasonic Wave Amplification and Improved Diagnostics". The support from the sponsoring organization is gratefully acknowledged.

References

Aggelis, D. G. and Matikas, T. E. (2012). "Effect of Plate Wave Dispersion on the Acoustic Emission Parameters in Metals," Computers & Structures, Vol. 98-99, pp. 17-22.

ASTM A572/A572M-18 Standard Specification for High-Strength Low-Alloy Columbium-Vanadium Structural Steel.

Bohlen, J., Chmelik, F., Dobron, P., Kaiser, F., Letzig, D., Lukac, P. and Kainer, K.U. (2004). "Orientation Effects on Acoustic Emission during Tensile Deformation of Hot Rolled Magnesium Alloy AZ31," Journal of Alloys and Compounds, Nol. 378, No. 1-2, 2004, pp. 207–213.

Botvina, L.R. and Tyutin, M.R. (2019). "New Acoustic Parameter Characterizing Loading History Effects," Engineering Fracture Mechanics, Vol. 210, pp. 358-366.

Jhang, K. Y., and Kim, K.C. (1999). "Evaluation of Material Degradation Using Nonlinear Acoustic Effect," Ultrasonics, Vol. 37, No. 1, 1999, pp. 39–44.

Jhang, K.Y. (2009). "Nonlinear Ultrasonic Techniques for Nondestructive Assessment of Micro Damage in Material: A Review," International Journal of Precision Engineering and Manufacturing, Vol. 10, No. 1, pp. 123–135.

Joseph, R., and Giurgiutiu, V. (2020). "Analytical and Experimental Study of Fatigue-Crack-Growth AE Signals in Thin Sheet Metals," Sensors, Vol. 20, No. 20, 5835.

Juliano, T. M., Meegoda, J. N., and Watts, D. J. (2013). "Acoustic Emission Leak Detection on a Metal Pipeline Buried in Sandy Soil," Journal of Pipeline Systems Engineering and Practice, Vol. 4, No. 3.

Kamali, N., Tehrani, N., Mostavi, A., Chi, S.W., Ozevin, D. and Indacochea, J.E. (2019). "Influence of Mesoscale and Macroscale Heterogeneities in Metals on Higher Harmonics Under Plastic Deformation," Journal of Nondestructive Evaluation, Vol. 38, No. 2. Kietov, V., Henschel, S. and Kruger, L. (2019). "AE Analysis of Damage Processes in Cast Iron and High-strength Steel at Different Temperatures and Loading Rates," Engineering Fracture Mechanics, Vol. 210, pp. 320-341.

Le Gall, T., Monnier, T., Fusco, C., Godin, N., and Hebaz, S.-E. (2018). "Towards Quantitative Acoustic Emission by Finite Element Modelling: Contribution of Modal Analysis and Identification of Pertinent Descriptors," Applied Sciences, Vol. 8, No. 12, 2557.

Lepikhin, A. M., Moskvichev, V. V., and Chernyaev, A. P. (2018). "Acoustic-Emission Monitoring of the Deformation and Fracture of Metal-Composite Pressure Vessels," Journal of Applied Mechanics and Technical Physics, Vol. 59, No. 3, pp. 511-518.

Li, W., Chen, B., Qing, X. and Cho, Y. (2019). "Characterization of Microstructural Evolution by Ultrasonic Nonlinear Parameters Adjusted by Attenuation Factor," Metals, Vol. 9, No. 3, 271.

Linderov, M.L., Segel, C., Weidner, A., Biermann, H. and Vinogradov, A.Y. (2018). "Study of Deformation Phenomena in TRIP/TWIP Steels by Acoustic Emission and Scanning Electron Microscopy," Physics of Metals and Metallography, Vol. 119, No. 4, pp. 388-395.

Lissenden, C. and Hasanian M. (2020). Chapter 3 – Measurement of Nonlinear Guided Waves. Measurement of Nonlinear Ultrasonic Characteristics. Springer Singapore.

Lyasota, I., Kozub, B. and Gawlik, J. (2019). "Identification of the Tensile Damage of Degraded Carbon Steel and Ferritic Alloy-steel by Acoustic Emission with in-situ Microscopic Investigations," Archives of Civil and Mechanical Engineering, Vol. 19, pp. 274-285.

Makhutov, N. A. (2019). "Acoustic Emission Analysis of Deformation and Damage Processes," Inorganic materials, Vol. 55, pp. 1511-1515.

Megid, W. A., Chainey, M. A., Lebrun, P., and Hay, R. D. (2019). "Monitoring Fatigue Cracks on Eyebars of Steel Bridges using Acoustic Emission: A Case Study," Engineering Fracture Mechanics, Vol. 211, pp. 198-208.

Merson, E.D., Myagkikh, P.N., Klevtsov, G.V., Merson, D.L. and Vinogradov, A. (2019). "Effect of Fracture Mode on Acoustic Emission Behavior in the Hyrogen Embrittled Lo-allow Steel," Engineering Fracture Mechanics, Vol. 210, pp. 342-357.

Mostavi, A., Kamali, N., Tehrani, N., Chi, S.W., Ozevin, D. and Indacochea, J.E. (2017). "Wavelet Based Harmonics Decomposition of Ultrasonic Signal in Assessment of Plastic Strain in Aluminum," Measurement, Vol. 106, pp. 66–78.

Ono, K. (2018). "Review on Structural Health Evaluation with Acoustic Emission," Applied Sciences, Vol. 8, No. 6, 958.

Penkin, A. G., Terent'ev, V. F., Roshchupkin, V. V., Slizov, A. K., and Sirotinkin, V. P. (2017). "Acoustic Emission Analysis of the Stages of Deformation of TRIP Steel," Russian Metallurgy, Vol. 2017, No. 4, pp. 306-311.

Petit, J., Montay, G. and Francois, M. (2018). "Strain Localization in Mild (Low Carbon) Steel Observed by Acoustic Emission – ESPI Coupling during Tensile Test," Experimental Mechanics, Vol. 58, pp. 743-758.

Qu, H., Li, T., Cain, J. A., and Chen, G. (2020). "Early Detection of Wire Fracture in 7-wire Strands through Multiband Wavelet Analysis of Acoustic Emission Signals," Engineering Structures, Vol. 207, 110227.

Quy, T. B., and Kim, J. M. (2020). "Leak Localization in Industrial-fluid Pipelines based on Acoustic Emission Burst Monitoring," Measurement, Vol. 151, 107150.

Solodov, I. (2020). Chapter 4: Nonlinear Acoustic Measurements for NDE Applications: Waves Versus Vibrations. Book Title Measurment of Nonlinear Ultrasonic Characteristics. Editors K.Y. Jhang, C.J. Lissenden, I. Solodov, Y. Ohara and V. Gusev. Springer.

Su, F., Li, T., Pan, X., and Miao, M. (2018). "Acoustic Emission Responses of Three Typical Metals During Plastic and Creep Deformations," Experimental Techniques, Vol. 42, No. 6, pp. 685-691.

Takemoto, M., Ueno, S., and Nakamura, M. (2017). "Source of AEs from IG-SCC of Face Centered Cubic Metals under Static or Dynamic Straining," Journal of Acoustic Emission, Vol. 34, S32.

Vinogradov, A. Y., and Merson, D. L. (2018). "The Nature of Acoustic Emission during Deformation Processes in Metallic Materials," Low Temperature Physics, Vol. 44, No. 9, pp. 930-937.

Vinogradov, A., Yasnikov, I. S., and Merson, D. L. (2019). "Phenomenological Approach towards Modelling the Acoustic Emission due to Plastic Deformation in Metals," Scripta Materialia, Vol. 170, pp. 172-176.

Viswanath, A., Rao, B. P. C., Mahadevan, S., Parameswaran, P., Jayakumar, T., Raj, B. (2011). "Nondestructive Assessment of Tensile Properties of Cold Worked AISI Type 304 Stainless Steel Using Nonlinear Ultrasonic Technique," Journal of Materials Processing Technology, Vol. 211, No. 3, pp. 538–544.

Yu, J., Ziehl, P., Zarate, B. and Caicedo, J. (2011). "Prediction of Fatigue Crack Growth in Steel Bridge Components using Acoustic Emission," Journal of Constructional Steel Research, Vol. 67, pp. 1254-1260.

Zhang, L., Oskoe, S. K., Li, H., and Ozevin, D. (2018). "Combined Damage Index to Detect Plastic Deformation in Metals Using Acoustic Emission and Nonlinear Ultrasonics," Materials (Basel), Vol. 11, No. 11, 2151.

Zhang, L., Zhang, T., Chen, E., Ozevin, D., and Li, H. (2020). "Phased Acoustic Emission Sensor Array for Localizing Radial and Axial Positions of Defects in Hollow Structures," Measurement, Vol. 151, 107223.

Zou, S. A., Yan, F. Y., Yang, G. A., and Sun, W. (2017). "The Identification of the Deformation Stage of a Metal Specimen Based on Acoustic Emission Data Analysis," Sensors, Vol. 17, No. 4, 13.